HHS Public Access

Author manuscript

Nature. Author manuscript; available in PMC 2020 February 05.

Published in final edited form as:

Nature. 2019 February ; 566(7745): 558–562. doi:10.1038/s41586-019-0949-1.

Multiplex Chromatin Interactions with Single Molecule Precision

Meizhen Zheng[1], **Simon Zhongyuan Tian**[1], **Daniel Capurso**[1], **Minji Kim**[1], **Rahul Maurya**[1], **Byoungkoo Lee**[1], **Emaly Piecuch**[1,2], **Liang Gong**[1], **Jacqueline Jufen Zhu**[1,2], **Zhihui Li**[1,3], **Chee Hong Wong**[1], **Chew Yee Ngan**[1], **Ping Wang**[1], **Xiaoan Ruan**[1], **Chia-Lin Wei**[1], **Yijun Ruan**[1,2,4,*]

[1]The Jackson Laboratory for Genomic Medicine, 10 Discovery Drive, Farmington, CT 06032, USA

[2]Department of Genetics and Genome Sciences, University of Connecticut Health Center, 400 Farmington Avenue, Farmington, CT 06030, USA

[3]School of Optometry and Ophthalmology, Wenzhou Medical University, Wenzhou, Zhejiang 325035, China

[4]Huazhong Agricultural University, Wuhan, Hubei 430070, China

Abstract

Genomes of higher organisms are extensively folded into three-dimensional (3D) chromosome territories within the nucleus[1]. Advanced 3D genome mapping methods that combine proximity ligation and high-throughput sequencing (Hi-C)[2], plus chromatin immunoprecipitation (ChIA-PET)[3], have revealed topologically associating domains (TADs)[4] with frequent chromatin contacts and have identified chromatin loops mediated by specific protein factors for insulation and transcriptional regulation[5–7]. However, these methods rely on pairwise proximity ligation and reflect population-level views, and thus cannot reveal the detailed nature of chromatin interactions. Although single-cell Hi-C[8] could potentially overcome this issue, it may be limited by data sparsity inherent to current single-cell assays. Recent advances in microfluidics have opened new opportunities for droplet-based genomic analysis[9], yet this approach has not been adapted to chromatin interaction analysis. Here, we describe a strategy for multiplex chromatin interaction analysis via droplet-based and barcode-linked sequencing (ChIA-Drop). We demonstrate the robustness of ChIA-Drop in capturing complex chromatin interactions with unprecedented single-

*Correspondence and requests for materials should be addressed to yijun.ruan@jax.org.

Author contribution

M.Z., Y.R., and C.L.W. conceptualized the ChIA-Drop strategy and designed the studies. M.Z. conducted experiments with assistance from Z. L., R.M., and C.Y.N. for ChIA-Drop library construction and sequencing. P.W., E.P., and J.J.Z. contributed RNAPII ChIA-PET data. X.R., D.C., and S.Z.T. contributed PacBio results. S.Z.T., M.K., D.C., and B.L. developed the computational pipeline ChIA-DropBox with C.H.W's assistance. M.Z. and Y.R. wrote the manuscript with input from D.C., M.K., S.Z.T., and B.L. All co-authors read and approved the manuscript.

Data Availability

The ChIA-Drop datasets, RNAPII ChIA-Drop datasets, RNAPII ChIA-PET datasets have been deposited in the Gene Expression Omnibus database with accession number GSE109355. A manuscript is in preparation on the ChIA-DropBox computational pipeline, and all software will be released as open-source code with that manuscript.

Online Content

Supplementary Methods, Supplementary Notes, Research reporting summaries, including statements of data availability and any associated accession codes and references, are available in the online version of the paper. Full statistics in Supplementary Methods.

The authors declare no competing interests.

molecule precision, which has not been possible with previous methods based on population-level pairwise contacts. Applying ChIA-Drop in *Drosophila* cells reveals that chromatin topological structures are predominantly comprised of multiplex chromatin interactions with high heterogeneity, and that promoter-centered multivalent interactions provide novel topological insights into transcription.

Reporting summary

Further information on research design is available in the Nature Research Reporting Summary linked to this paper.

To develop ChIA-Drop, we used *Drosophila* S2 cells, a well-characterized model[10], and adopted the Chromium microfluidics system (10X Genomics), which was established for high-molecular-weight genomic DNA[9]. In ChIA-Drop, a crosslinked and fragmented chromatin sample is directly loaded to the microfluidics device without proximity ligation or DNA purification. Each chromatin complex is partitioned in a Gel-bead-in-Emulsion (GEM) droplet that contains unique DNA oligonucleotides and reagents for linear amplification and barcoding. The barcoded amplicons with GEM-specific indices are then pooled for high-throughput sequencing, and the sequencing reads with identical barcodes are computationally assigned to the same GEM of origin. Mapping of the sequencing reads to the reference genome identifies which remote genomic loci are in close spatial proximity. Thus, multiplex chromatin interactions can be inferred (Fig. 1a). We optimized and verified that this microfluidic-based approach can produce high-quality and reproducible data directly from the crosslinked chromatin sample (Supplementary Methods, Supplementary Table 1; Extended Data Fig. 1–2).

Concurrently, we developed a comprehensive analysis and visualization pipeline, ChIA-DropBox (Supplementary Note 1). From sequencing reads, ChIA-DropBox first identifies the droplet barcode (GEMcode). After mapping, high-quality reads with same GEMcode are grouped, and overlapping reads are merged to represent DNA fragments. Fragments tagged with same GEMcode are assumed to originate from the same GEM, ideally from a single chromatin complex tethering multiple distal DNA fragments. Due to randomness of the emulsion process of droplet formation, multiple chromatin complexes could potentially be partitioned into the same GEM. Given that most chromatin contacts are intra-chromosomal, chromatin complexes of inter-chromosomal origins in a GEM can be separated computationally into intra-chromosomal sub-GEMs, representing putative chromatin complexes. For example, in one ChIA-Drop dataset of 5.7 million chromatin fragments assembled from 51 million reads, we identified 1.2 million intra-chromosomal putative complexes from 1.6 million GEMs (Supplementary Note 1). A major source of noise was singleton DNA fragments, which are readily filtered out in downstream analysis. Furthermore, we developed a “domain-based distance test” algorithm based on polymer physics[11] and information theory[12] to further characterize intra-chromosomal complexes (Supplementary Note 1).

In theory, ChIA-Drop should detect the same spectrum of chromatin contacts as Hi-C. To compare ChIA-Drop with Hi-C data[13], we devised an *in silico* ligation algorithm to generate

pairwise contacts from ChIA-Drop data (Supplementary Note 1) and show that their chromatin structural features are comparable (Fig. 1b–c, Extended Data Fig. 2d). Unlike Hi-C, ChIA-Drop can resolve the multiplex nature of chromatin interactions. Indeed, about half (n=1,493,818) of ChIA-Drop complexes contained three or more fragments, some (n=19,778) even had up to hundreds of chromatin fragments (Supplementary Table 2). We decomposed the ChIA-Drop data based on fragment numbers and visualized each class separately with 2D maps. Most of the contacts from low-fragment-number complexes (F=2–5) appeared randomly scattered, whereas high-fragment-number complexes tended to cluster into distinct topological structures along the diagonal (Fig. 1d, Extended Data Fig. 2g), which was also observed in the cumulative distribution of pairwise distances by fragment number (Fig. 1e, Extended Data Fig. 2h).

We then focused on high-fragment-number ChIA-Drop complexes (F≥6; n=170,752) for further analysis. We visualized these complexes in their linear alignment along genomic bins, with complexes organized by similarity along the y-axis via hierarchical clustering (Fig. 2a; Supplementary Note 1). Notably, the fragment clusters were closely associated with topological domains, indicating that single-molecule ChIA-Drop complexes provided genuine information on chromatin conformation. ChIA-Drop complexes associated with TADs contained more fragments on average than those associated with gap regions (Fig. 2a, Extended Data Fig. 2i–j). Overall, 85% (82,506) of ChIA-Drop complexes associated with TADs fall within a single TAD, though 15% (14,630) cover several TADs (Fig. 2b). Many of these inter-TAD interactions (4,757 of 9,723) were significant by a “frequency-based binomial test”, suggesting higher-order chromatin organization (Supplementary Note 1). Therefore, our ChIA-Drop data demonstrate extensive multiplexity of chromatin interactions inside and between TADs.

We validated the single-molecule multiplex nature of ChIA-Drop complexes using an orthogonal protocol based on PacBio long-read sequencing of proximity-ligated chromatin fragments (Supplementary Methods). Although most of the long-reads included only one chromatin fragment, we identified thousands that included multiple fragments and showed high heterogeneity within TADs, similar to the intra-TAD ChIA-Drop data (Extended Data Fig. 3a–b).

Additionally, we applied 4-color 3D FISH to confirm the inter-TAD multiplexity of the ChIA-Drop complexes. For a genomic segment (1.1 Mb) in chr2L that contains three interacting TADs and one non-interacting TAD, we designed fluorescent DNA probes corresponding to the 4 TAD regions (Fig. 2c), where probe **T2*** was expected to be an internal negative control, and two T4 probes (T4a and T4b) served as intra-TAD references. As expected, the spatial distance measured by FISH between T4a and T4b was small (mode = 0.22 μm) (Fig. 2d, Extended Data Fig. 3k). The spatial distance of T1-T4b was substantially shorter than the distance of **T2***-T4b, even though **T2*** is closer in linear genomic distance. We defined FISH signals as “colocalized” based on a distance cutoff (0.28 μm), and calculated the percentage of colocalization for two- and three-probe combinations and compared these with ChIA-Drop complexes. Overall, the FISH patterns and colocalization percentages were highly consistent with ChIA-Drop (Fig. 2d–e). Additional

FISH validations also supported the observed ChIA-Drop interactions[14,15] (Extended Data Fig. 3c–j).

Most ChIA-Drop TADs in *Drosophila* S2 cells were closely associated with repressed chromatin, whereas boundary gaps were transcriptionally active (Fig. 2f, Extended Data Fig. 2d–e), consistent with previously reported findings[16]. Additionally, two architectural proteins had interesting binding patterns: BEAF-32[17] tended to define TAD boundaries, whereas Su(Hw)[18] tended to occur within TADs, potentially for heterochromatin compaction (Fig. 2g). Together, ChIA-Drop data revealed a single-molecule view of complex chromatin contacts represented individually in many cells, instead of the topological approximation based on aggregated pairwise contacts from bulk cells (Fig. 2h).

We next investigated multiplex chromatin interactions involved in transcriptional regulation by adding RNAPII chromatin immunoprecipitation to the ChIA-Drop protocol (Fig. 1a; Supplementary Methods). Replicates of RNAPII ChIA-Drop were high-quality and reproducible (Supplementary Table 1; Extended Data Fig. 2a), with 80% of chromatin contacts (frequency count ≥ 3) observed across replicates (Extended Data Fig. 4e). We identified ~2 million chromatin complexes in S2 cells by RNAPII ChIA-Drop ($F \geq 2$) (Supplementary Table 1 and 3). In general, RNAPII ChIA-Drop recapitulated similar topological structures as ChIA-Drop, but, as expected, exhibited considerable signal reduction in repressed domains (TADs) and enrichment in active regions (boundary gaps) (Fig. 3a).

We then compared RNAPII ChIA-Drop to RNAPII ChIA-PET. In RNAPII ChIA-PET data, transcriptionally active regions often contain interconnected daisy-chain loops referred to as RNAPII-associated interaction domains (RAIDs) (Supplementary Note 1, Supplementary Table 1; Extended Data Fig. 5). Using RNAPII ChIA-PET data, we called 476 RAIDs in S2 cells (Supplementary Table 4, Supplementary Note 2). We converted RNAPII ChIA-Drop data to pairwise loops, which were mostly enriched in RAIDs, with some inter-RAID contacts as also seen in RNAPII ChIA-PET and in Kc167 cells[16] (Fig. 3b, Extended Data Fig. 6).

We validated the multiplex RNAPII ChIA-Drop complexes using 4-color 3D FISH. In a chromatin segment (1.12 Mb) in chr2L, RNAPII ChIA-Drop complexes connected several RAIDs for which we designed 4 probes (Fig. 3c). Since RNAPII-mediated chromatin architectures in *Drosophila* are sensitive to heat-shock (HS)[19], we used HS treatment as a negative control. As expected, in many normal cells the probes were spatially colocalized, whereas in most HS cells the probes were scattered (Fig. 3d–e, Extended Data Fig. 3l). Thus, the RNAPII ChIA-Drop data, including the 16 chromatin complexes involving 3 RAIDs in this region (Fig. 3c), are likely to reflect true multiplex chromatin interactions in single molecules.

Next, we analyzed the multiplexity of chromatin complexes by comparing to a binomial model of expected interaction complexity (Supplementary Note 2). Overall, the multiplexity of chromatin complexes in RAIDs was lower than expected, whereas that in TADs was higher (Extended Data Fig. 6j–k). We also quantified the heterogeneity of multiplex

chromatin complexes in RAIDs and in TADs, which may reflect cell-to-cell variation (Supplementary Note 2). Chromatin interactions within RAIDs and TADs are both heterogeneous, though to a higher degree in TADs (Fig. 3f, top). The subset of complexes in RAIDs that involve promoters tends to be less heterogeneous (Fig. 3f, bottom), suggesting possible exclusivity behavior of promoter-involving interactions. A similar level of heterogeneity was observed by single-cell RNA-Seq (Fig. 3f, bottom), indicating a commonality with transcriptional function.

The multiplex single-molecule complexes from RNAPII ChIA-Drop provide an unprecedented opportunity to explore topological mechanisms of transcription, which led us to focus on complexes involving promoters in RAIDs ($F \geq 2$; n=175,294). Notably, 80% of such RNAPII complexes included only one promoter (Fig. 4a). For instance, an active region including *luna* and *Shn* genes had interconnected daisy-chain loops in RNAPII ChIA-PET data (Extended Data Fig. 8a) and in pairwise loops of the RNAPII ChIA-Drop data (Fig. 4b), but the single-molecule fragment views of the RNAPII ChIA-Drop revealed that promoters are rarely interconnected (Fig. 4b; Extended Data Fig. 7a). This suggest that in individual cells most promoters are not spatially inter-connected (Fig. 3b; Extended Data Fig. 7a). Nonetheless, we still captured more than 2,700 complexes that simultaneously connected at least three promoters (Supplementary Note 2; Fig. 4a), supporting the notion that multiplex promoter interactions occur in single molecules, but not as extensively as previously suggested[5].

To explore the properties of co-transcriptionally regulated genes[5], we focused on RNAPII ChIA-Drop complexes involving 3 promoters and obtained 4 clusters based on gene expression (Supplementary Table 5, Supplementary Note 2; Extended Data Fig. 7b). Group I and group II are imbalanced with 1 and 2 dominant gene(s), respectively, while groups III and IV are balanced with three equally expressed genes. This suggests at least two different mechanisms for transcription coordination: “co-transcription” (groups III and IV), where all the promoters are active, and “imbalanced-transcription” (groups I and II), where promoters of weak genes behave like enhancers to support the expression of the dominant genes as previously postulated[5]. Indeed, the weak promoters exhibited a enhancer-like status, as measured by the ratio of H3K4me/me3 ChIP-Seq signals (Fig. 4c, Extended Data Fig. 7c–e).

RNAPII ChIA-Drop data also revealed abundant intragenic contacts with orientation biased towards the downstream direction of transcription (Fig. 4b, Extended Data Fig. 7f), particularly for large genes over 100 Kb length such as *luna*[20]. An aggregation plot for all promoter-involving RNAPII ChIA-Drop complexes along a normalized gene body model (Supplementary Note 2) demonstrates that, genome-wide, intragenic chromatin contacts are directionally biased toward the transcriptional end site (TES) (Fig. 4d). At the *luna* gene locus (Fig. 4e), RNAPII ChIA-PET data displayed a remarkable chromatin contact “stripe” starting from the promoter, suggesting a likely transcriptional processivity of chromatin looping. RNAPII ChIA-Drop identified 87 complexes involving the *luna* promoter, of which the majority (72; 83%) extended downstream from TSS towards TES, where each of the RNAPII ChIA-Drop complexes represents a possible chromatin looping structure anchored at the promoter site (Fig. 4f, Extended Data Fig. 8).

The orientation-bias pattern may potentially support a one-sided extrusion model for transcription, which is different from a conventional tracking model[21]. Here, we envision that the RNAPII protein cluster with co-factors is assembled at the promoter site, or that gene promoters are attracted to RNAPII clusters. When transcription starts, the promoter site is in steady position, while the DNA template is reeled through the transcriptional apparatus for RNA synthesis. Interestingly, in chromatin complexes containing fewer fragments, the chromatin contacts were a short distance from the *luna* promoter, reflecting the starting phase of DNA extrusion and the formation of small loops. In larger complexes (more fragments), there were more chromatin contacts far away from the promoter and closer to TES, indicating more complicated chromatin looping structures (inset of Fig. 4f).

In summary, ChIA-Drop is a simple, robust and effective method for capturing multiplex chromatin interactions at the single-molecule level, an advance over previous pairwise, population-level methods like Hi-C and ChIA-PET. The protocol requires only ~5×10^3 cells, or ~6×10^4 cells for a ChIP-enriched experiment. We anticipate that ChIA-Drop will be rapidly adopted for a wide range of biomedical questions and applications. We demonstrated in S2 cells that TADs are composed of interactions with high complex-to-complex heterogeneity, analogous to the dynamics reported using a super-resolution imaging approach in single cells[22]. More importantly, we characterized transcriptional multiplex interactions. Contrary to previous population-level analyses that suggested extensive promoter-promoter interactions[5], RNAPII ChIA-Drop data revealed that 80% of transcriptionally-active chromatin complexes involve interactions of only one promoter with non-promoter distal elements, consistent with recent studies using super-resolution microscopy of RNAPII foci[23,24]. The 20% of chromatin complexes involving multiple promoters support the idea of transcription factories[25], but that these may not be as prevalent as previously suggested[5]. We provided evidence for at least two putative mechanisms of transcriptional coordination: co-transcription and imbalanced-transcription. Moreover, we detected processive multiplex chromatin contacts connected to active gene promoters in the direction of transcriptional orientation, and accordingly we propose a promoter-centered one-sided extrusion model for RNAPII-mediated transcription.

Extended Data

a **Pure DNA vs Chromatin DNA**

	Pure DNA	Chromatin DNA
Total reads	2,545,248	2,191,091
GEM barcode with reads	**1,064,328**	**686,493**
Reads with GEM barcode	2,355,569	1,970,016
Uniquely mapped reads	2,261,170	1,155,343
Uniquely mapped reads (%)	**95.99%**	**58.65%**

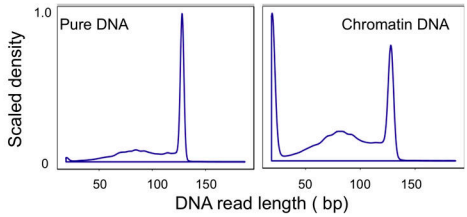

b

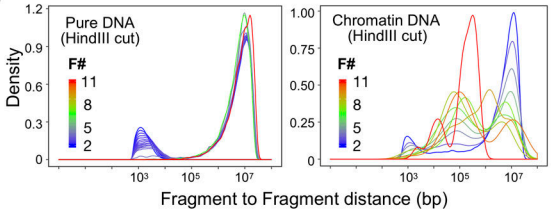

c

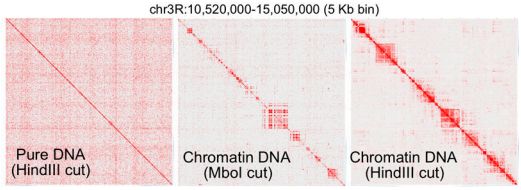

d **Different chromatin fragment length**

	4 bp cutter (MboI)	6 bp cutter (HindIII)	Sonication
Total reads	4,656,784	4,868,248	2,274,570
GEM barcode with reads	**845,883**	**1,044,653**	**748,048**
Reads with GEM barcode	4,216,577	4,460,036	2,043,330
Uniquely mapped reads	1,782,446	3,178,376	1,517,719
Uniquely mapped reads (%)	**42.27%**	**71.26%**	**74.28%**

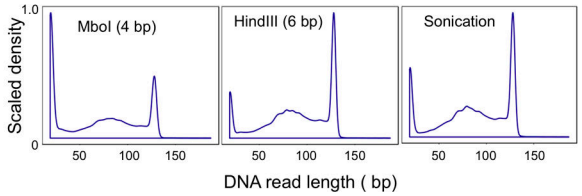

e **Sequencing data of MboI vs HindIII cuts**

	4 bp cutter (MboI)	6 bp cutter (HindIII)
Total reads	98,399,745	105,814,667
Reads with GEM barcode	87,779,074	95,271,125
GEM barcode	**1,919,641**	**1,914,282**
Uniquely mappable reads	39,246,891	65,051,724
Uniquely mappable reads (%)	**44.70%**	**68.30%**
F = 1	616,750	1,837,201
F = 2	40,401	406,107
F = 3	4,594	100,538
F = 4	1,112	29,781
F = 5	466	11,347
F = 6	287	5,350
F = 7	164	3,089
F = 8	104	1,944
F = 9	77	1,312
F = 10	73	944
F = 11	51	728
F = 12	41	592
F = 13	33	474
F = 14	23	399
F = 15	26	329
F > 15	151	2,522

f **Different loading quantity of chromatin DNA**

	0.5 ng	0.5 pg
Total reads	2,274,570	1,780,274
GEM barcode with reads	**748,048**	**519,010**
Reads with GEM barcode	2,043,330	1,601,257
Uniquely mapped reads	1,517,719	456,471
Uniquely mapped reads (%)	**74.28%**	**28.51%**

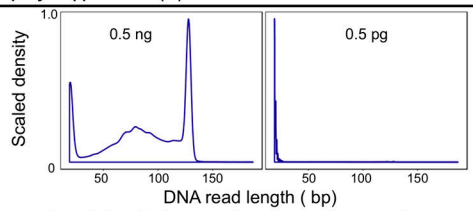

g **Sequencing data of Inter-species chromatin samples**

***Drosophila* : Human**	Cell # (1:1)	Chromatin (1:1)
Total reads	1,992,569	4,656,784
GEM barcode with reads	669,843	845,883
Reads with GEM barcode	1,809,743	4,216,577
Uniquely mapped reads	808,269	1,782,446
GEM with fragments	192,377	279,127
Drosophila	9,149	142,975
(%)	4.76%	51.22%
Human	181,956	121,920
(%)	94.58%	43.68%
Inter-species	1,272	14,232
(%)	**0.66%**	**5.10%**

Extended Data Figure 1. ChIA-Drop method optimization.

The efficiency of the microfluidics system for chromatin DNA barcoding and amplification was characterized by MiSeq sequencing data, where each test generated 2–4 million sequencing reads. The numbers of captured GEM barcodes, the percentages of uniquely mapped reads, and the read length distribution are presented for data quality assessment. **a** Pure DNA versus chromatin DNA. Both pure DNA and chromatin DNA templates were prepared from the same chromatin sample. The chromatin sample was prepared by *in situ* HindIII digestion followed by sonication for nuclear lysis. The chromatin DNA used for test was still in crosslinked state, and some DNA positions were bound by protein component. The pure DNA was purified from the chromatin fragment after de-crosslinking. The length of the DNA templates was about 3,000 bp. Most of the pure DNA sequencing reads were in

maximum length (130 bp), of which 96% were mappable. The chromatin DNA yield 59% mappable reads.

b Distance density comparison of pure DNA and chromatin DNA. The relative probability densities of the log10 of fragment-to-fragment distances in a GEM are plotted, categorized by the fragment number per GEM (F#), color code blue-green-red for fragment F=2, F=3, up to F=11. Both pure DNA (left) and chromatin DNA (right) data are plotted on the same color scale. To be noted, the low-fragment-containing GEMs showed the similar distributions as the pure DNA, whereas the chromatin DNA with high-fragment-containing GEMs displayed different patterns.

c 2D heatmap comparison of pure DNA (HindIII, 6-bp cutter), chromatin DNA (Mbol, 4-bp cutter and HindIII). The pure DNA data show random interactions and lack chromatin topological structures; the Mbol chromatin DNA data exhibit little structures, and HindIII chromatin DNA data show rich chromatin contact structures.

d Chromatin fragment length by different fragmentation methods. Chromatin sample digested by 4bp-cutter (MboI, ~300 bp) or 6bp-cutter (HindIII, ~3,000 bp), or sheared by sonication (~6,000 bp) were prepared accordingly. The longer chromatin fragments (3,000–6,000 bp) generated more mappable DNA sequencing reads (≥50 bp) than the shorter fragments.

e Summary statistics of GEMs from chromatin libraries prepared by Mbol and HindIII digestion. The read statistics between the two libraries are comparable under the same loading amount, but the fragment histograms of GEMs are different. The HindIII data generated more uniquely mappable reads and more high-fragment-containing GEMs than the Mbol data, contributing to the chromatin structures shown in (c).

f Chromatin sample loading by different input quantity. Input chromatin DNA of 0.5 ng yield optimal results. When input was too low (i.e., 0.5 pg), the majority of the sequencing reads were only 19–20 bp (barcode primer sequence), indicating that most droplets lack chromatin materials.

g Inter-species chromatin experiment. Chromatin samples of *Drosophila* S2 and human GM12878 cells were mixed in equal number of cells or in equal quantity of chromatin DNA. Barcoded sequencing reads were mapped to each reference genome. Reads with the same GEMbarcode were grouped as a GEM. GEMs with fly-only, human-only, or mixed reads were identified. The ratio of mixed GEMs over the total GEMs is an approximate likelihood of a mixed chromatin complex in a droplet. When tested with equally mixed numbers of cells, the number of GEMs with chromatin fragments of human origin is 20-fold more than GEMs of *Drosophila* origin (181,956 / 9,149 = 19.89), which reflect the ratio of human to *Drosophila* genome lengths (hg 3,000 Mb / dm 175 Mb = 17.14). Notably, in the test with equal chromatin mass, the GEMs with mixed origins of fragments were only 5.1%, indicating a small proportion of droplets with mixed chromatin samples.

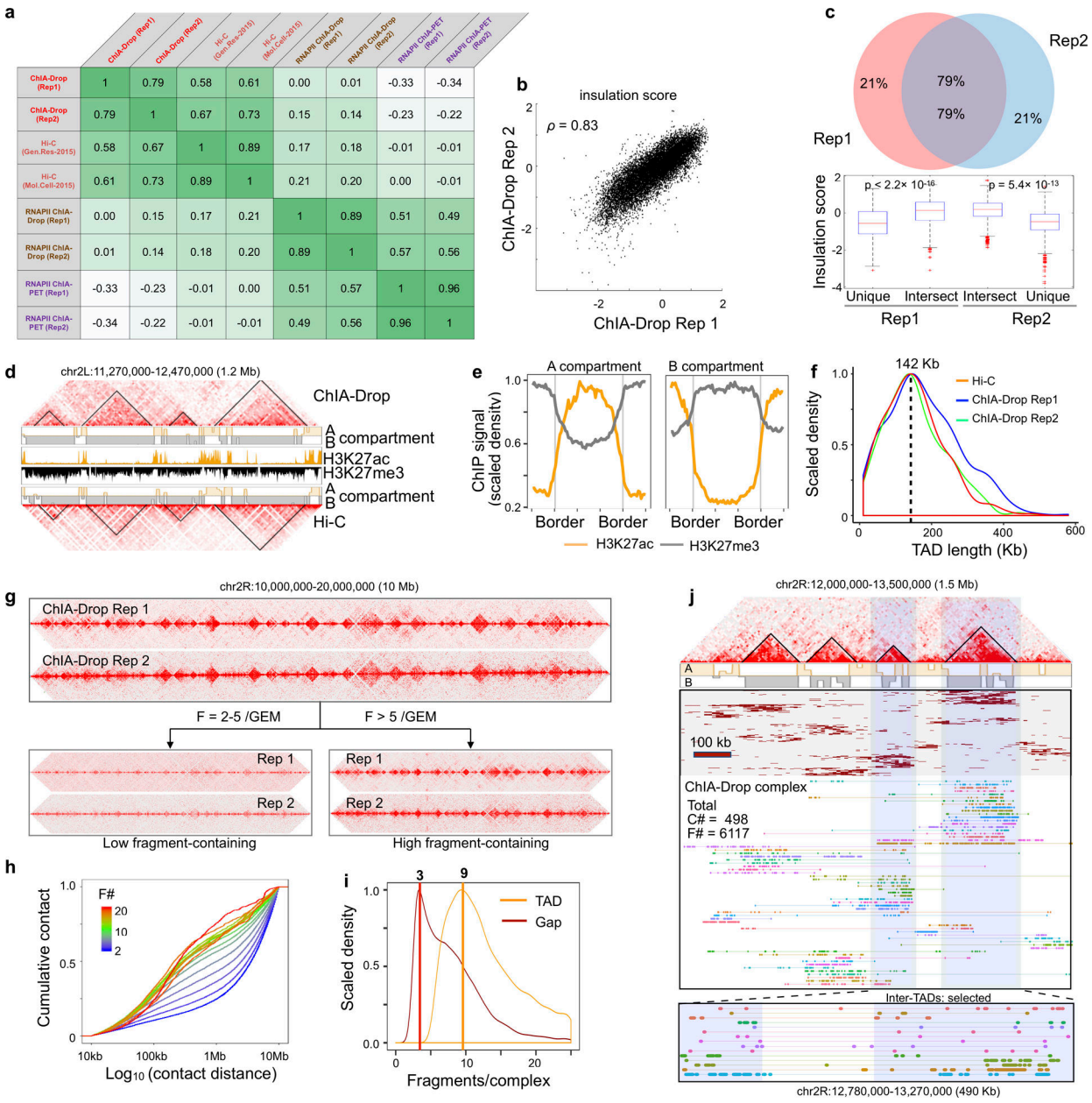

Extended Data Figure 2. ChIA-Drop data reproducibility and characterization.

a Genome-wide reproducibility assessment of ChIA-Drop and RNAPII ChIA-Drop. To best assess the data quality and reproducibility, we conducted a comprehensive comparison between 4 datasets (ChIA-Drop, Hi-C, RNAPII ChIA-Drop, and RNAPII ChIA-PET), each with two replicates for reproducibility analysis using HiCRep. Each row and column represent the 8 datasets of interest, and the entry indicates the correlation coefficient ('scc' output from HiCRep) between the corresponding row and column. The entries are color-coded by their values, with darker colors for higher values.

b Scatter plot of insulation scores between ChIA-Drop replicates. The insulation scores of every 10 kb bins (n=11,918) are computed and plotted genome-wide for both replicates of ChIA-Drop, with Spearman correlation coefficient $\rho = 0.83$.

c Venn diagram of TAD comparison between ChIA-Drop Rep1 and Rep2. Of 471 and 522 TADs called from Rep1 and Rep2 respectively, 79% overlapped. Boxplots of insulation scores for reproducible TADs and replicate-specific TADs show that the reproducible TADs have higher scores (boxplot: middle line, median; box, interquartile range (IQR); whiskers, 1.5xIQR). The unique and intersect parts with either replicates show high differences (two-sided Wilcoxon test p-value < 2.2×10^{-16} for Rep1, and p-value = 5.42×10^{-13} for Rep2). Details in the Supplementary Methods.

d Browser view of A/B compartment and TAD of ChIA-Drop and Hi-C data. For a given 1.2 Mb window, ChIA-Drop and Hi-C data heatmaps are presented along with their TADs (triangle) and A (light orange)/B (grey) compartments by eigenvectors, and histone ChIP-seq H3K27ac (golden) and H3K27me3 (black) tracks. Both ChIA-Drop and Hi-C data exhibit similar patterns.

e Epigenomic patterns in A and B compartments. Each of the A and B compartments is binned to 300 bins and are extended by 100 bins on both ends. The RPM scaled densities of H3K27ac and H3K27me3 ChIP-seq signals are plotted.

f TAD size distribution. From Hi-C and two replicates of ChIA-Drop data, TADs are called via insulation scores. The resulting densities of TAD sizes (lengths) are plotted, with a peak at 142 Kb for all three datasets.

g 2D contact map of two replicates of ChIA-Drop data. A 10 Mb region is shown for two replicates in contact heatmaps. HiCRep correlation coefficient, scc = 0.79.

h Distribution of contact distances by fragment size. The empirical cumulative distribution function (ECDF) of log10 of contact distances support the observed pattern that small complexes have larger contact distances than large complexes, where the color bar scales from blue, green to red for fragments in ascending order. F#: Fragment number per complex.

i Distribution plots for the number of fragments per chromatin complex involved in TADs or in gap regions.

j A zoomed-in browser view (1.5 Mb) showing that ChIA-Drop complex clusters associate with TADs. From top to bottom, ChIA-Drop 2D pairwise contact map showing a region with a number of TADs and boundary regions; eigenvector-called A/B (orange/gray, respectively) compartments from ChIA-Drop data; cluster view of the chromatin complexes in this region with binning at 10Kb resolution; fragment view of the chromatin complexes in this region. Each set of the assorted color bars connected by a straight line depicts a ChIA-Drop chromatin complex. A further zoomed-in fragment view (490 Kb), highlighting the inter-TAD chromatin complexes, was shown at the bottom.

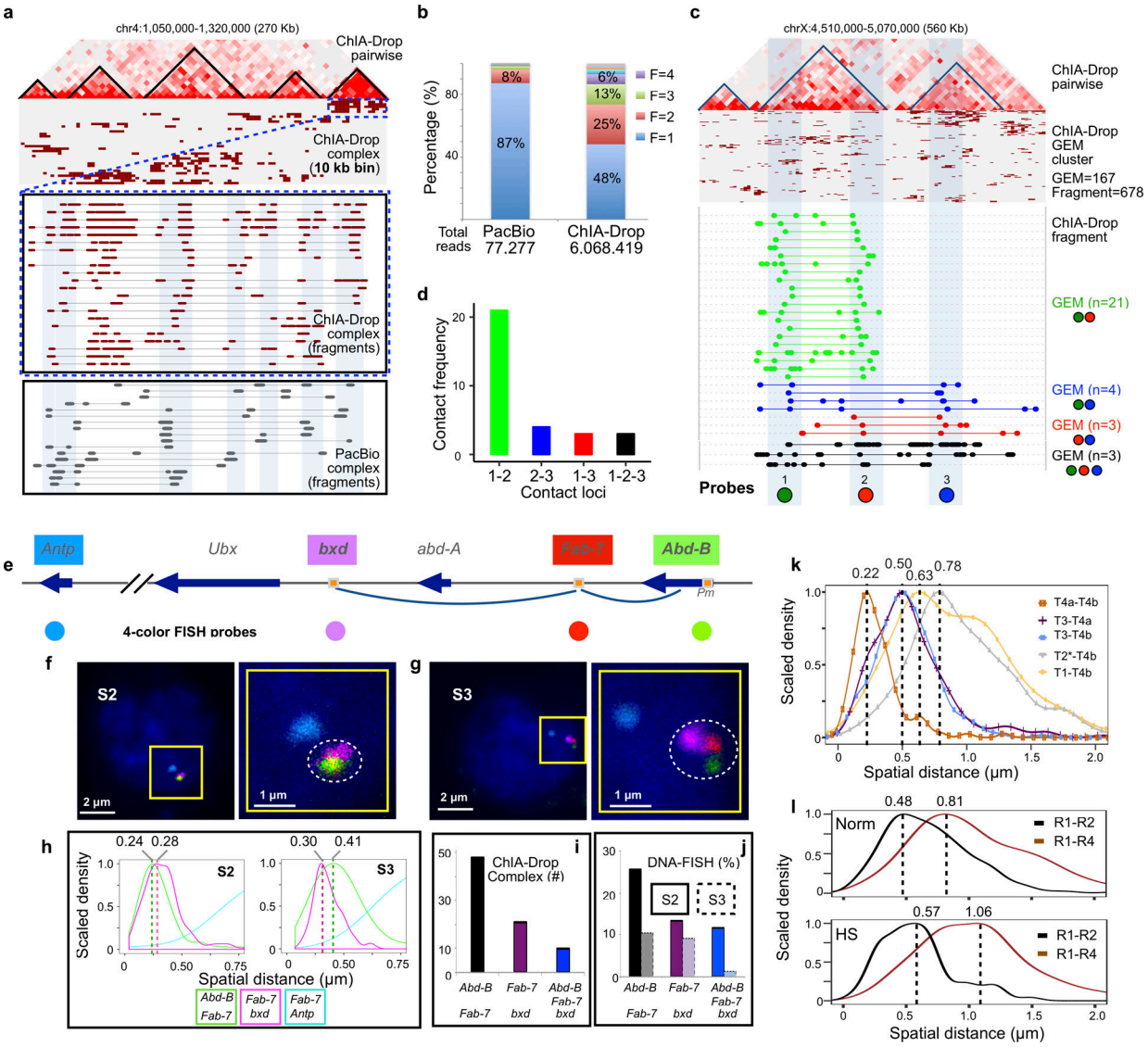

Extended Data Figure 3. Technical validation of ChIA-Drop data.

a Comparison of ChIA-Drop and PacBio detected multiple chromatin complexes. In a given 270 Kb window, a linear fragment view of ChIA-Drop data shows clusters associated with TAD structures. A zoomed-in view displays the overlapping chromatin fragments from ChIA-Drop and PacBio complexes, with matching regions highlighted in light blue. Both complex data exhibit high level of heterogeneity.

b Comparison of distributions of fragment number in chromatin complexes in PacBio and ChIA-Drop data. Both methods captured multiplex chromatin complexes at a single-molecule resolution. Under the same cost, PacBio sequencing generated less number of reads than ChIA-Drop sequencing using Miseq. With more reads, ChIA-Drop data show higher multiplexity in chromatin contacts than PacBio data.

c ChIA-Drop data of chromatin contacts with multiple fragments were shown in pairwise 2D contact map, complex cluster, and fragment views in this region. The same region was studied by Szabo and colleagues[15] using 3D super-resolution DNA-FISH (3D-SIM), with

three probes (1 ‘green’, 2 ‘red’, 3 ‘blue’) designed to test intra-TAD contacts (probe 1–2) and inter-TAD contacts (probe 1–3, 2–3, and 1-2-3). ChIA-Drop detected all combinations possible pairwise and 3-way contacts, and the number of GEMs are noted as n.

d ChIA-Drop contact frequencies between the 3 loci are plotted. The highest contacts were between the intra-TAD loci 1 and 2, and the 3 other combinations of inter-TAD were low approximately at the same level. The intra-TAD and inter-TAD contact frequencies matched with the physical distances of the three loci as measured by 3D-SIM. More specifically, individual GEMs contained fragments that overlap the 3 probed loci were detected, validating ChIA-Drop for detecting multiplex chromatin contacts.

e Diagram of Hox genes cluster BX-C (bithorax complex, comprises three Hox genes, *Ubx*, *abd-A*, and *Abd-B*). The pairwise chromatin contacts between *Fab-7*|*Abd-B* and *Fab-7*|*abd-A* were shown by 2-color FISH in S2 cells but not in S3 cells. The three loci, *bxd*, *Fab-7* and the *Abd-B* promoter (Pm), were used to make fluorecent DNA probes as shown. *Fab-7* and *bxd* are separated by approximately 130 kb, *Fab-7* and *Abd-B* Pm by approximately 70 kb. Gene *Antp* in another Hox gene cluster ANT-C (Antennapedia complex) approximity 10 Mb away from BX-C was also included for a fluorecent probe to provide a nuclear position point in FISH experiment. An arrow indicates gene orientation, square with orange color indicates promoter regulatory elements (PRE), and the colored circle dots represent DNA probes with corresponding colors.

f Four-color FISH in *Drosophila* S2 cells. The three loci (*Abd-B*, *Fab-7*, and *bxd*; n=20, measured in 179 nuclei from two independent biological replicates) were colocalized, and the probe for *Antp* locus provided spatial nuclear position. The scale bar is either 2 μm or 1 μm as indicated. Right side is zoom-in view of the left side.

g Four-color FISH in *Drosophila* S3 cells. The three loci (*Abd-B*, *Fab-7*, and *bxd*; n=1, measured in 76 nuclei from two independent biological replicates) were notably not colocalized, revealing topological structure of of this Hox gene cluster. Same as in S2 cell, the probe for *Antp* locus provided spatial nuclear position.

h Curves of spatial distances (μm) between pairs of probes measured by Imaris image analysis software v9.2. The modes of the distances of *Abd-B* to *Fab-7* is 0.24 μm in S2 cells (n = 179) and 0.41 μm in S3 cells (n = 76); the modes of the distances of *Fab-7* to *bxd* is 0.28 μm in S2 cells (n = 179), and 0.3 μm in S3 cells (n = 76). In both cells, the modes of the distances of *Fab-7* to *Antp*, are larger than 1.81 μm.

i Histogram displays the ChIA-Drop-identified chromatin contacts at the Hox gene locus between *Abd-B* to *Fab-7*, *Fab-7* to *bxd*, and *Abd-B* to *Fab-7* to *bxd* together simultaneously.

j Histogram displays proportions of nuclei that were detected colocalization at loci between *Abd-B* to *Fab-7*, *Fab-7* to *bxd*, and *Abd-B* to *Fab-7* to *bxd* together simultaneously. With spatial distance cutoff of 0.24 μm, the more nuclei colocalized in S2 cells (n = 179) than in S3 cells (n = 76).

k Distributions of spatial distances (μm) between pairs of probes, measured using the Imaris image analysis software. The modes of the distance distributions for each pair of probes are as follows: T4a-T4b, mode Mo = 0.22 (nuclei, n = 221); T3-T4a, Mo = 0.5 (nuclei, n = 221); T3-T4b, Mo = 0.5 (nuclei, n = 404); T2*-T4b, Mo = 0.78 (nuclei, n = 404); T1-T4b, Mo = 0.63 (nuclei, n = 404).

l Spatial distances (μm) of probe pairs in normal S2 cells (n = 213) and heat-shock (HS) treated cells (n = 150), analyzed using the Imaris image analysis software. Upper panel,

distributions of spatial distances in the normal, untreated cells (n = 213). The modes of spatial distance distributions for each of the probe pairs are: R1-R2, mode Mo = 0.48; R1-R4, Mo = 0.81. Lower panel, curves of spatial distances in the heat-shock treated cells (n = 150). The modes of spatial distance distributions for each of the probe pairs are: R1-R2, Mo = 0.57; R1-R4, Mo = 1.06. The spatial distances of R1-R2 and R1-R4 observed in HS treated cells were notably larger than in untreated normal cells.

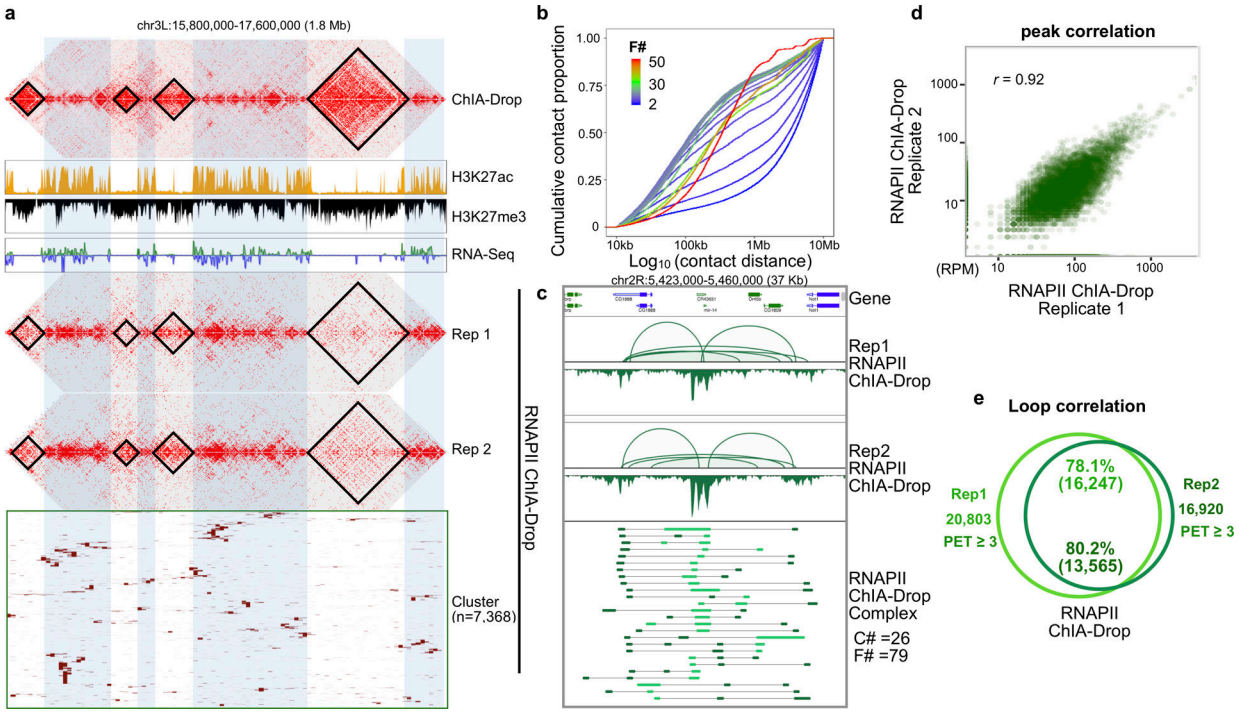

Extended Data Figure 4. Characterization of RNAPII ChIA-Drop data.

a Comparison of 2D contact maps between ChIA-Drop and RNAPII ChIA-Drop replicates (Rep1 and Rep2) in a 1.8 Mb segments in chr 3L. TADs called in ChIA-Drop are shown in 2D contact maps, along with tracks of histone marks H3K27ac, H3K27me3 and RNA-Seq to illustrate the active and inactive regions. Complex Cluster of RNAPII ChIA-Drop data are shown at the bottom. Notably, contact signals in RNAPII ChIA-Drop data were enriched in active regions but reduced in inactive regions.

b Distribution of contact distances by GEM complexity of fragment numbers. The empirical cumulative distribution function (ECDF) of log10 of contact distances support the pattern that small complexes have larger contact distances than large complexes. Color scales for each curve were from the spectrum of blue to green to red for fragment numbers 2 to 30 to 50 in ascending order. F#: Fragment number per complex.

c Basic browser view in a 37 Kb window (chr2R:5,423,000–5,460,000) to display the loops and peaks from two replicates of RNAPII ChIA-Drop data. Multiple ChIA-Drop fragments (n = 79) of chromatin complexes (n = 26) were shown in the bottom panel.

d Scatter plot shows peaks (n = 14,347) correlation between two replicates inside RAID regions. Pearson correlation coefficient $r = 0.92$.

e Venn diagram shows the loop anchor overlapping between two replicates inside RAID regions. Loop numbers with PET counts cutoff were indicated.

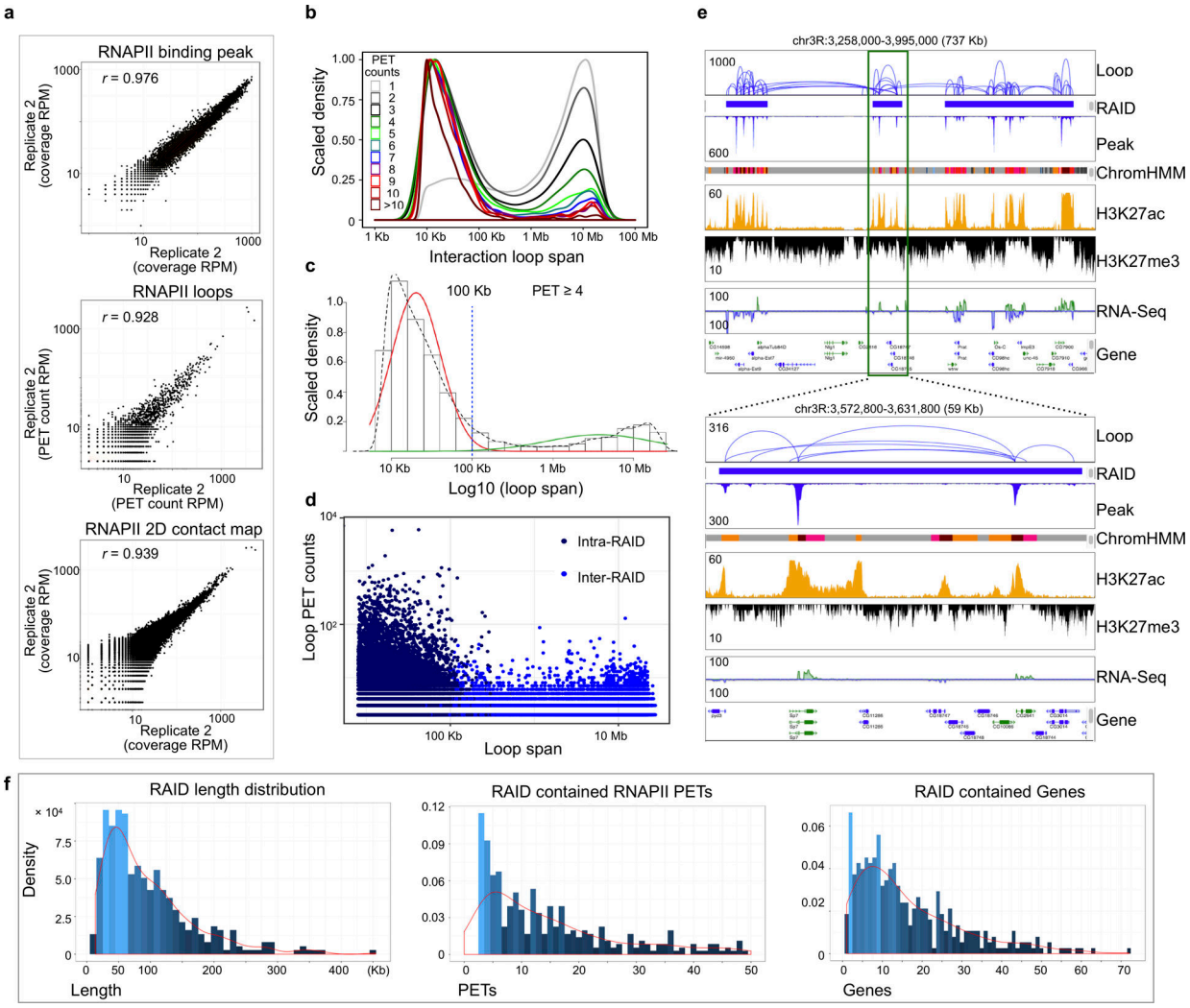

Extended Data Figure 5. Characterization of RNAPII ChIA-PET data.

a Correlation of RNAPII ChIA-PET data between two replicates. Scatterplot shows two replicates of RNAPII ChIA-PET data, peak coverage (RPM, top, n = 5,924 union peaks), loops frequency (RPM, middle, n = 23,773 overlapped loops), and 2D contact map (100 kb/bin, RPM, bottom, n=1,449,616 bins). Pearson correlation coefficient are $r = 0.976$, $r = 0.928$ and $r = 0.939$ from top to bottom panels, respectively.

b Loop span distribution by PET counts. The interaction loop spans (n= 1,461,514) are recorded separately by the PET counts and their distributions are plotted. Those with high PET counts tend to have shorter loop spans than those with low PET counts. Colors denote PET counts.

c Mixture model for loop span. The population of loops (n = 17,088 loops) is separated into mid-range interaction (red) and long-range interaction (green) classes through the Gaussian mixture model. Dotted line shows the marginal distribution of the log10(loop span) for loops with ≥ 4 PET counts, and 100 Kb is selected as a cutoff threshold.

d Relationship between loop size and PET counts with respect to RAIDs. Loops (n = 90,885, PET ≥ 2) are categorized into intra-RAID (n = 476 RAIDs) if both anchors are in the

same RAID and inter-RAID if they span two different RAIDs. The log of loop size and log of PET counts are plotted, with colors indicating the two categories.

e Browser view. A 737 Kb region is presented along with RAIDs, epigenomic-defined states (ChromHMM, color codes indict 9 chromatin state), and various ChIP-seq and RNA-Seq signal tracks. Daisy-chain like loops tend to be clustered inside a RAID, but long-range inter-RAID loops also exist. A 59Kb RAID region is highlighted below.

f Characteristics of RAIDs (n=476). The lengths, loop PET counts, and gene counts in RAIDs are plotted as histograms and density lines.

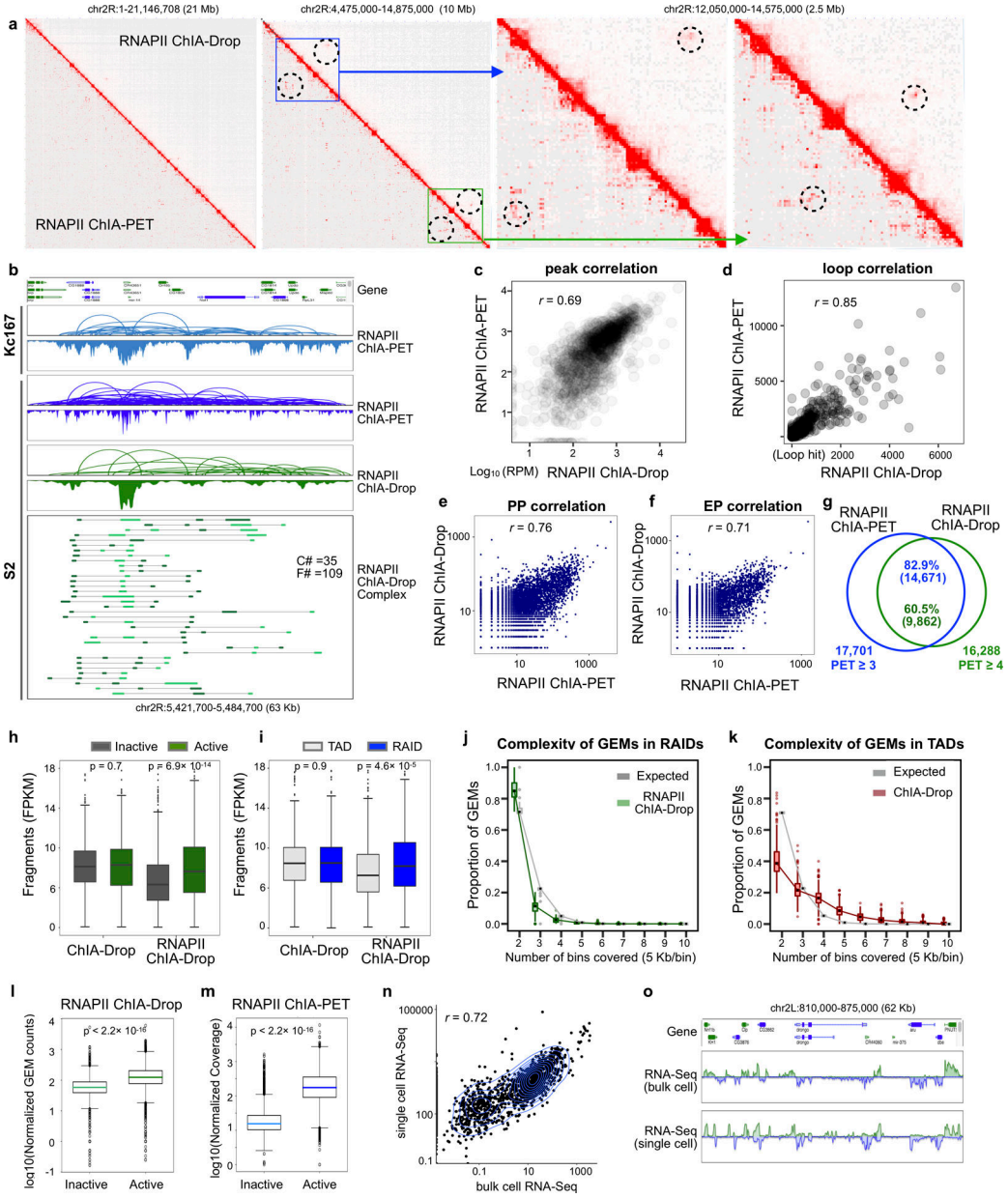

Extended Data Figure 6. Comparison of RNAPII ChIA-PET RNAPII ChIA-Drop.

a 2D contact maps comparison. The 2D contact maps of RNAPII ChIA-PET (lower left) and RNAPII ChIA-Drop (upper right) are displayed at multiple resolutions (whole chromosome 2R, a 10 Mb segment, and two 2.5 Mb domains). Dotted circles highlight the long-range loops identified by both methods.

b Loops, peaks and fragment visualization. In a 63 Kb window in chr2R, the RNAPII ChIA-PET loops and peaks are similar for Kc167 and S2 cell lines. Moreover, the RNAPII ChIA-Drop data in loop and peaks veiw are in high concordance with the RNAPII ChIA-PET loops in S2 cells. Individual complexes with multiplex fragments show further details of RNAPII ChIA-Drop data. C#: complex number; F#: fragment number.

c Peak correlation. Taking all peaks called by RNAPII ChIA-PET and RNAPII ChIA-Drop inside RAIDs (n = 476), the signal density of peak unions (n = 1,521) in RPM are plotted in log10 scale. Pearson correlation coefficient $r = 0.69$.

d Loop count correlation. The number of loops in corresponding RAIDs (n = 476) identified in RNAPII ChIA-Drop and RNAPII ChIA-PET data were counted for each RAID. The loop counts of each RAID were ploted. Pearson correlation coefficient $r = 0.85$.

e Promoter-to-promoter (PP) correlation. For each gene promoter (n = 9,133 genes with PP interaction), the number of interactions with another promoter were counted in both RNAPII ChIA-PET and RNAPII ChIA-Drop data and are plotted in log10 scale. Pearson correlation coefficient $r = 0.76$.

f Promoter-to-enhancer (PE) correlation. Each gene promoter (n = 7,115 genes with PE interaction) is evaluated for its interactions with enhancers (i.e., 'non-TSS') and the counts are plotted (Pearson correlation coefficient $r = 0.71$).

g Loop anchor correlation. Venn diagram shows that 82.9% of the RNAPII ChIA-PET loops with PET ≥ 3 within RAIDs overlap with 60.5% of the RNAPII ChIA-Drop loops with PET ≥ 4 inside RAIDs.

h Boxplot of normalized ChIA-Drop fragment coverage in chromatin domains. Left panel: the coverage in active domains (dark green) and inactive domains (dark gray) from ChIA-Drop data or RNAPII-enriched ChIA-Drop data. The active/inactive domains were called by segmenting signals for RNA-Seq and histone modification ChIP-seq (Inactive Domains, $n = 706$; Active Domains, $n = 708$; ChIA-Drop, two-sided Wilcoxon test p-value = 0.72; RNAPII_ChIA-Drop, p-value = 6.94×10^{-14}). For each box plot, the middle line indicates the median, the shaded box indicates the IQR (interquartile range), and the whiskers extend to a max of 1.5 × IQR beyond the box. Data points are plotted as dots individually if they are located beyond ends of the whiskers. Details in the Supplementary Methods.

i Boxplot of coverage in chromatin domains (boxplot: middle line, median; box, interquartile range (IQR); whiskers, 1.5xIQR). The coverage in TADs (silver) and RAIDs (blue) from ChIA-Drop data or RNAPII ChIA-Drop data (TADs, $n = 583$; RAIDs, $n = 476$; ChIA-Drop, two-sided Wilcoxon test p-value = 0.97; RNAPII ChIA-Drop, p-value = 4.61×10^{-5}). RAIDs are chromosome regions defined by merging high confidential loops (PET ≥ 4, span ≤ 100 kb) from RNAPII ChIA-PET data (Supplementary Methods). TADs were called by calculating insulation score. Detailed statistics in the Supplementary Methods.

j Boxplot of the complexity of RNAPII ChIA-Drop chromatin complexes in RAIDs (boxplot: middle line, median; box, interquartile range (IQR); whiskers, 1.5xIQR). RAIDs (n = 476) are binned at 5 Kb resolution and the number of bins covered by each chromatin complex in RNAPII ChIA-Drop data is counted. Individual distributions across each RAID are averaged, with the heights indicating the means and the error bars indicating one standard deviation. The gray bar shows an expected random distribution based on a binomial model, and yellow dots are individual data points. Chromatin complexes from RNAPII ChIA-Drop in RAIDs show lower complexity than expected (i.e., more constrained).

k The complexity boxplot of ChIA-Drop significant chromatin complexes in TADs (boxplot: middle line, median; box, interquartile range (IQR); whiskers, 1.5xIQR). TADs ($n = 582$) are binned at 5 Kb resolution and the number of bins covered by each chromatin complex in ChIA-Drop data is counted. Barplots follow the same convention as panel (j), but unlike in

(j), chromatin complexes from ChIA-Drop in TADs show higher complexity than expected (Supplementary Note 2).

l Bias towards active genes in RNAPII ChIA-Drop. The number of chromatin complexes (GEM) overlapping with active (n = 7,334) and inactive (n = 3,210) gene promoters inside RAIDs are recorded and are normalized by the number of unique isoforms (Supplementary Methods). The boxplot shows a preference towards active genes (boxplot: middle line, median; box, interquartile range (IQR); whiskers, 1.5xIQR). Two-sided Wilcoxon test p-value < 2.2×10^{-16}. Detailed statistics in the Supplementary Methods.

m Bias towards active genes in RNAPII ChIA-PET. Instead of the GEM counts in ChIA-Drop (panel d), the coverage in ChIA-PET are recorded and normalized accordingly. The skew towards active genes are yet again observed (n = 7,334 active genes and n = 3,210 inactive genes) in the boxplot (boxplot: middle line, median; box, interquartile range (IQR); whiskers, 1.5xIQR). Two-sided Wilcoxon test p-value < 2.2×10^{-16}. Detailed statistics in the Supplementary Methods.

n Single cell RNA-Seq (scRNA-Seq) and bulk cell RNA-Seq correlation. Using the RPKM of single cell RNA-Seq cell and bulk RNA-Seq expression level for genes in S2 (n = 2,094 genes), the two sets of numbers are plotted in log10 scale (Pearson correlation coefficient r = 0.72).

o Single cell RNA-Seq (scRNA-Seq) and bulk cell RNA-Seq visualization. The bulk RNA-Seq expression level and the accumulated scRNA-Seq expressed level show similar profile.

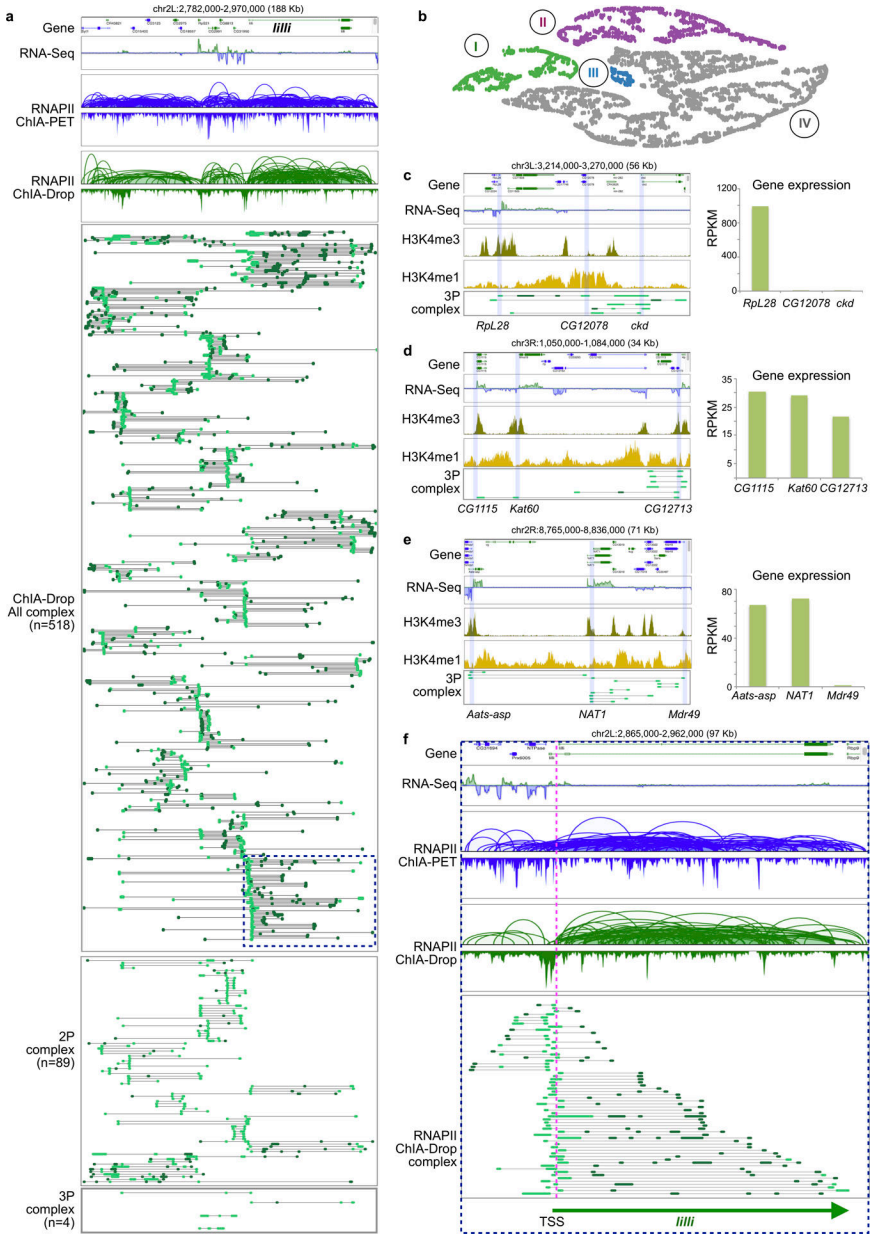

Extended Data Figure 7. Examples of RNAPII ChIA-Drop data.

a Promoter-centric view of RNAPII ChIA-Drop complexes at the 188 kb region with 28 genes including *lilli*, a large gene of length 65 Kb. This region contains 518 promoter-linked complexes including one-promoter complexes (1P complex, $n = 425$), two-promoter complexes (2P complexes, $n = 89$), and three-promoter complexes (3P complexes $n = 4$). 2P and 3P complexes are shown in the lower panel.

b Among the chromatin complexes involving three promoters (3P), different subgroups were identified based on expression levels of the three genes. Each chromatin complex is displayed as a dot, arranged by similarity via dimensionality reduction and density based clustering (Supplementary Methods). Clusters are color-coded.

c 3-gene complex with one dominant gene. RNAPII ChIA-drop connected promoters of 3 genes *RpL28*, *CG12078*, and *ckd*. Based on the RNA-seq and histone marks, only *RpL28* displays active behaviors. The expression level (in RPKM) of the three genes are shown as a bar chart.

d 3-gene complex with three dominant genes. All three genes, *CG1115*, *Kat60*, and *CG12713* -- simultaneously captured by RNAPII ChIA-Drop-- are active with similarly high expression levels.

e 3-gene complex with two dominant genes. Only *Aats-asp* and *NAT1* are active, with *Mdr49* potentially playing the role of an enhancer (expression level on the right).

f An example of intra-genic RNAPII ChIA-Drop data. At the *lilli* locus, processive promoter-linked multiplex chromatin contacts covering the entire gene body are shown. The number of fragments in a complex reflects potential looping complexity for the one-sided extrusion model in transcription.

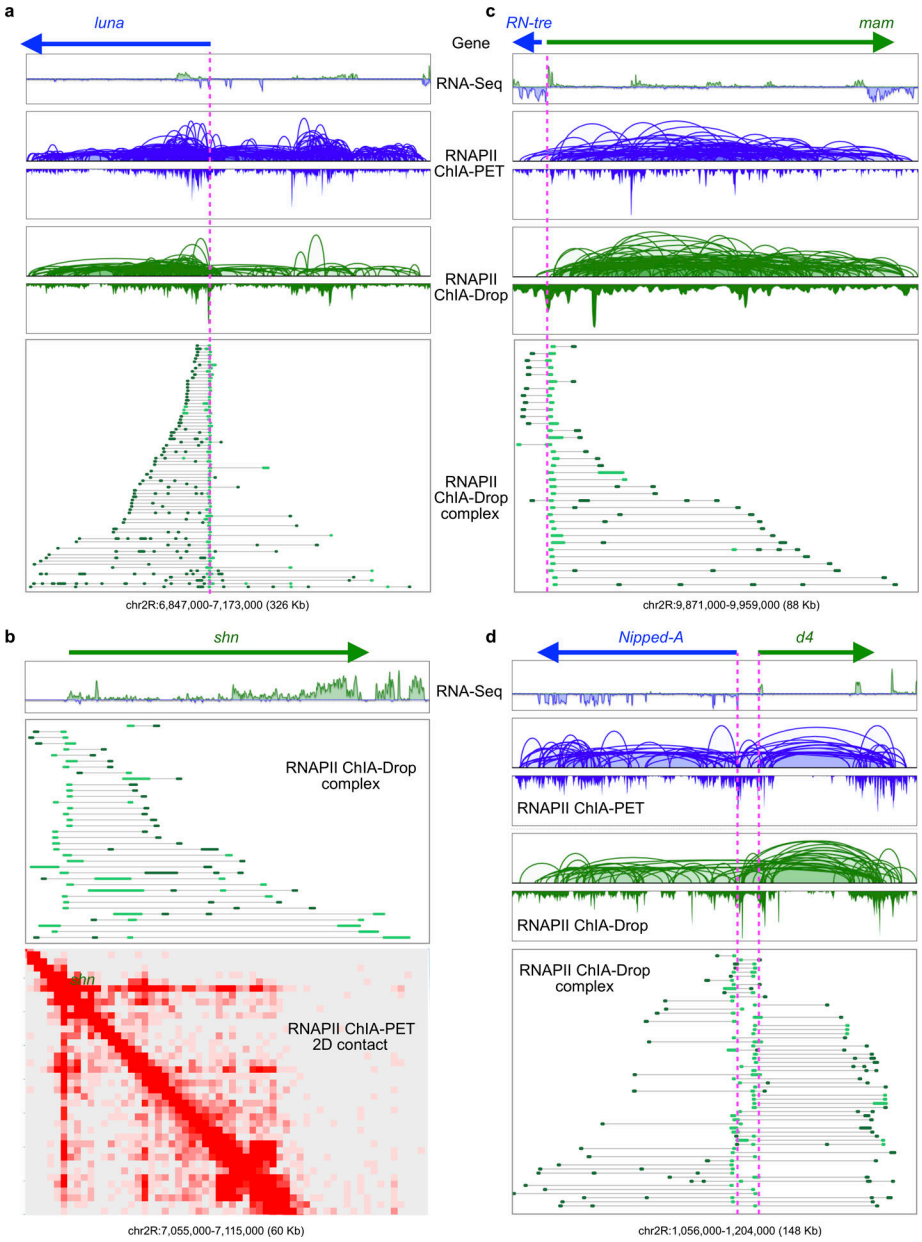

Extended Data Figure 8. Examples of RNAPII ChIA-Drop data.

a Browser view of *luna* gene. Processive promoter-linked multiplex chromatin contacts covering the entire *luna* gene body are shown. Only a few chromatin contacts appear in the upstream of the *luna* gene, indicating the specific chromatin interactions in the direction of gene transcription.

b Browser view of *shn* gene. Similar to *luna*, the *shn* locus displays processive promoter-linked multiplex chromatin contacts. Also, 2D contact maps of RNAPII ChIA-PET show chromatin contact “stripe” pattern supporting the RNAPII ChIA-Drop data.

c Processive promoter-linked multiplex chromatin contacts at the *mam* locus.

d Processive promoter-linked multiplex chromatin contacts at the locus of *Nipped-A* and *d4* genes in the opposite transcription direction.

Supplementary Material

Refer to Web version on PubMed Central for supplementary material.

Acknowledgments

This study is supported by a Jackson Laboratory Director's Innovation Fund (DIF19000-18-02). Y.R. and C.L.W. are funded by 4DN (U54 DK107967) and ENCODE (UM1 HG009409) consortia. Y.R. is also funded by Human Frontier Science Program (RGP0039/2017), and supported by Florine Roux Endowment.

Reference

1. Cremer T & Cremer M Chromosome territories. Cold Spring Harbor perspectives in biology 2, a003889, doi:10.1101/cshperspect.a003889 (2010). [PubMed: 20300217]
2. Lieberman-Aiden E et al. Comprehensive mapping of long-range interactions reveals folding principles of the human genome. Science 326, 289–293, doi:10.1126/science.1181369 (2009). [PubMed: 19815776]
3. Fullwood MJ et al. An oestrogen-receptor-alpha-bound human chromatin interactome. Nature 462, 58–64, doi:10.1038/nature08497 (2009). [PubMed: 19890323]
4. Dixon JR et al. Topological domains in mammalian genomes identified by analysis of chromatin interactions. Nature 485, 376–380, doi:10.1038/nature11082 (2012). [PubMed: 22495300]
5. Li G et al. Extensive promoter-centered chromatin interactions provide a topological basis for transcription regulation. Cell 148, 84–98, doi:10.1016/j.cell.2011.12.014 (2012). [PubMed: 22265404]
6. Tang Z et al. CTCF-Mediated Human 3D Genome Architecture Reveals Chromatin Topology for Transcription. Cell 163, 1611–1627, doi:10.1016/j.cell.2015.11.024 (2015). [PubMed: 26686651]
7. Weintraub AS et al. YY1 Is a Structural Regulator of Enhancer-Promoter Loops. Cell 171, 1573–1588 e1528, doi:10.1016/j.cell.2017.11.008 (2017). [PubMed: 29224777]
8. Nagano T et al. Single-cell Hi-C reveals cell-to-cell variability in chromosome structure. Nature 502, 59–64, doi:10.1038/nature12593 (2013). [PubMed: 24067610]
9. Zheng GX et al. Haplotyping germline and cancer genomes with high-throughput linked-read sequencing. Nature biotechnology 34, 303–311, doi:10.1038/nbt.3432 (2016).
10. Kharchenko PV et al. Comprehensive analysis of the chromatin landscape in Drosophila melanogaster. Nature 471, 480–485, doi:10.1038/nature09725 (2011). [PubMed: 21179089]
11. Lajoie BR, Dekker J & Kaplan N The Hitchhiker's guide to Hi-C analysis: practical guidelines. Methods 72, 65–75, doi:10.1016/j.ymeth.2014.10.031 (2015). [PubMed: 25448293]
12. Cover TM & Thomas JA Elements of Information Theory. 2 edn, (John Wiley & Sons, 2006).
13. Ulianov SV et al. Active chromatin and transcription play a key role in chromosome partitioning into topologically associating domains. Genome research 26, 70–84, doi:10.1101/gr.196006.115 (2016). [PubMed: 26518482]
14. Lanzuolo C, Roure V, Dekker J, Bantignies F & Orlando V Polycomb response elements mediate the formation of chromosome higher-order structures in the bithorax complex. Nature cell biology 9, 1167–1174, doi:10.1038/ncb1637 (2007). [PubMed: 17828248]
15. Szabo Q et al. TADs are 3D structural units of higher-order chromosome organization in Drosophila. Science advances 4, eaar8082, doi:10.1126/sciadv.aar8082 (2018). [PubMed: 29503869]
16. Rowley MJ et al. Evolutionarily Conserved Principles Predict 3D Chromatin Organization. Molecular cell 67, 837–852 e837, doi:10.1016/j.molcel.2017.07.022 (2017). [PubMed: 28826674]
17. Yang J, Ramos E & Corces VG The BEAF-32 insulator coordinates genome organization and function during the evolution of Drosophila species. Genome research 22, 2199–2207, doi:10.1101/gr.142125.112 (2012). [PubMed: 22895281]

18. van Bemmel JG et al. The insulator protein SU(HW) fine-tunes nuclear lamina interactions of the Drosophila genome. PloS one 5, e15013, doi:10.1371/journal.pone.0015013 (2010). [PubMed: 21124834]
19. Cai W et al. RNA polymerase II-mediated transcription at active loci does not require histone H3S10 phosphorylation in Drosophila. Development 135, 2917–2925, doi:10.1242/dev.024927 (2008). [PubMed: 18667461]
20. Duff MO et al. Genome-wide identification of zero nucleotide recursive splicing in Drosophila. Nature 521, 376–379, doi:10.1038/nature14475 (2015). [PubMed: 25970244]
21. Alberts B, Johnson A, Lewis J, Raff M, Roberts K and Walter P. Molecular biology of the cell. 4 edn, (Garland Science, 2002).
22. Bintu B et al. Super-resolution chromatin tracing reveals domains and cooperative interactions in single cells. Science 362, doi:10.1126/science.aau1783 (2018).
23. Cisse II et al. Real-time dynamics of RNA polymerase II clustering in live human cells. Science 341, 664–667, doi:10.1126/science.1239053 (2013). [PubMed: 23828889]
24. Zhao ZW. Spatial organization of RNA polymerase II inside a mammalian cell nucleus revealed by reflected light-sheet superresolution microscopy. Proceedings of the National Academy of Sciences of the United States of America; 2014. 681–686.
25. Cook PR A model for all genomes: the role of transcription factories. Journal of molecular biology 395, 1–10, doi:10.1016/j.jmb.2009.10.031 (2010). [PubMed: 19852969]

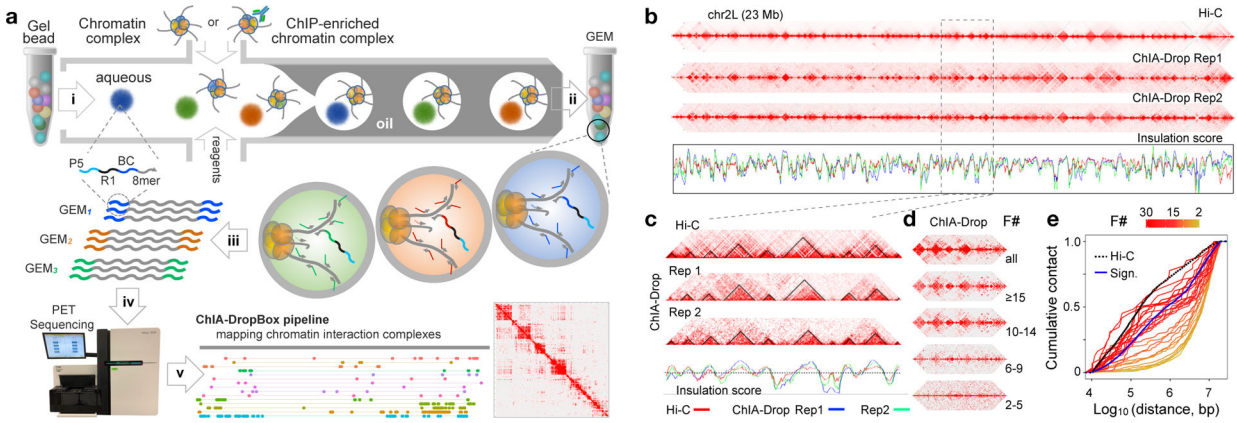

Figure 1. ChIA-Drop overview

a. ChIA-Drop schematic. i) Chromatin samples or ChIPed samples are loaded to the device to produce Gel-bead-in-Emulsion (GEM) droplets, each with a unique barcode ("P5", PCR priming site; "R1", sequencing priming site; "BC", 16-nt barcode; "8-mer", random 8-nt). ii) DNA templates in GEMs are annealed for linear amplification and barcoding. iii) Barcoded amplicons are pooled for iv) sequencing and v) mapping *via* ChIA-DropBox pipeline for visualizations.

b. Comparing Hi-C and ChIA-Drop. Insulation scores (red: Hi-C; blue: Rep1; green: Rep2) have Spearman correlation of 0.84 (Rep1 vs. Rep2), 0.60 (Rep1 vs. Hi-C), and 0.72 (Rep2 vs. Hi-C).

c. Zoomed view (2.1 Mb) of panel (**b**). Spearman correlation of insulation scores: 0.87 (Rep1 vs. Rep2), 0.77 (Rep1 vs. Hi-C), and 0.84 (Rep2 vs. Hi-C).

d. ChIA-Drop data (chr2R:19.1–20.1Mb): all complexes and then complexes decomposed by fragment number (*F*).

e. Cumulative distribution for the pairwise distances of ChIA-Drop interactions, plotted by fragment number (*F*) (Blue: significant ChIA-Drop data; black dotted, Hi-C data).

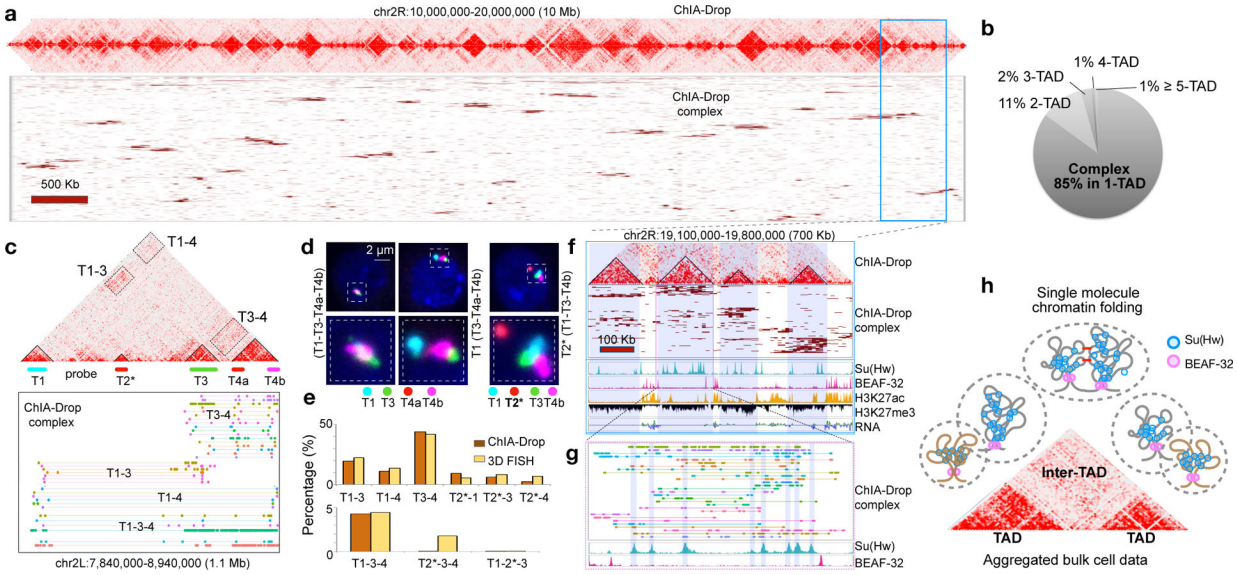

Figure 2. Multiplex chromatin interactions from ChIA-Drop

a. ChIA-Drop data shown as "linear multi-fragment views" of complexes with ≥10 fragments. Each row is a complex and columns are 50 Kb bins.

b. Proportion of chromatin complexes in single TAD (1-TAD) or multiple TADs (2- to 5-TAD).

c. ChIA-Drop data containing 4 TADs. Fluorescent DNA probes T1-T4b were designed.

d. FISH images. *Left*, 4 test probes colocalized (T1-T3-T4a-T4b) in 17 of 404 nuclei; *middle*, 3 test probes colocalized (T3-T4a-T4b) in 177 of 404 nuclei; *right*, the control **T2*** probe far from the other probes in 221 of 221 nuclei. Data are combined from two replicates.

e. Percentage of ChIA-Drop complexes involving a given combination of TADs and the corresponding FISH colocalization (*Top*, 2-TADs; *Bottom*, 3-TADs). 150 nuclei were analyzed with a 0.28 μm "colocalization" cutoff.

f. A 700 kb region in chr2R shows ChIA-Drop complexes binned at 10 kb, along with RNA-Seq and ChIP-Seq of Su(Hw), BEAF-32, H3K27ac, and H3K27me3.

g. Further zoom of chromatin complexes (n=29) with their fragments (n=328) (*top*), along with Su(Hw) and BEAF-32 profiles (*bottom*).

h. Proposed single-molecule model of chromatin folding in topological domains. BEAF-32 defines TAD boundaries. Within domains, chromatin is folded randomly and associated with Su(Hw). Nearby domains likely have random or specific inter-domain contacts (red bars).

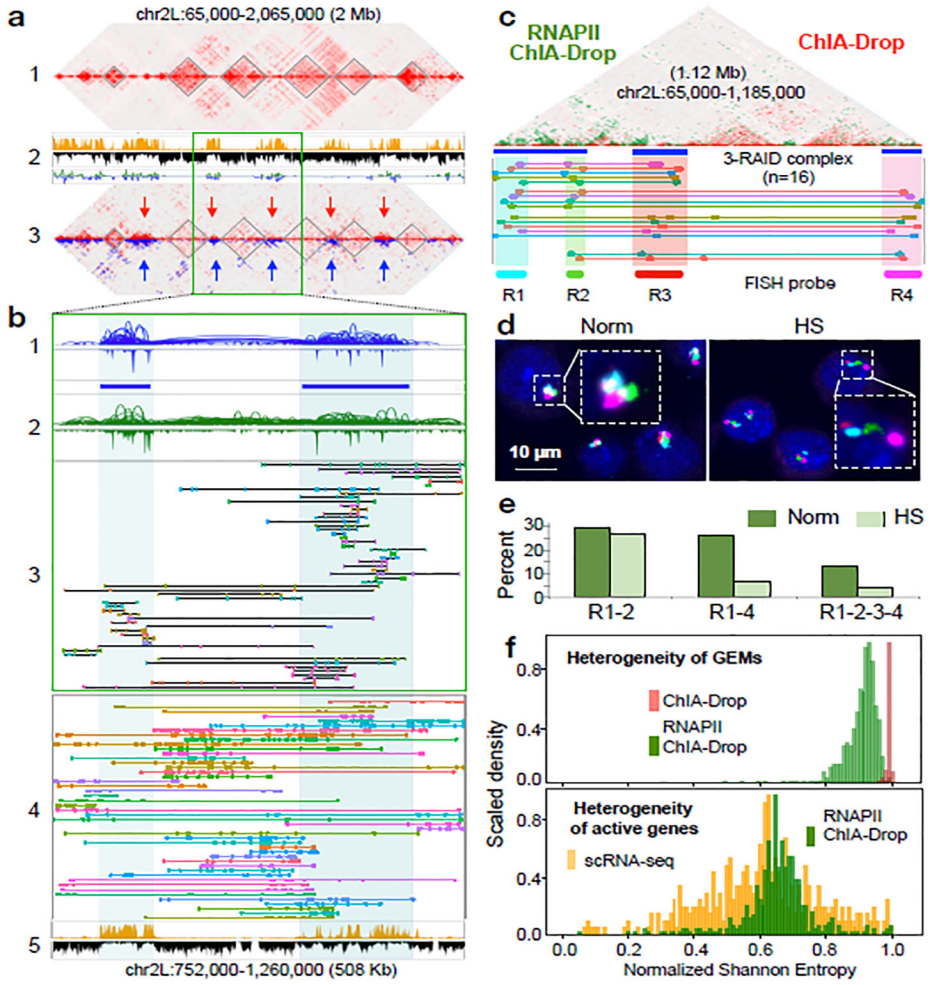

Figure 3. Characterization of RNAPII ChIA-Drop

a. ChIA-Drop data shows a number of TADs and gap regions (Track-1), along with H3K27ac/me3 and RNA-Seq signals (Track-2). Track-3 shows RNAPII ChIA-Drop contacts (red) superimposed with chromatin loops (blue) identified by RNAPII ChIA-PET. Red and blue arrows indicate loci with enriched signals.

b. A zoomed-in view of a 508 Kb segment from (**a**). From top to bottom: 1) RNAPII ChIA-PET loops and peaks in two RAIDs (blue); 2) RNAPII ChIA-Drop loops and peaks (green); 3) RNAPII ChIA-Drop multiplex ($F \geq 5$) complexes ($n=64$) and fragments ($n=454$) are shown; 4) ChIA-Drop multiplex ($F \geq 10$) complexes ($n=48$) and fragments ($n=814$) are shown; 5) H3K27ac/me3.

c. ChIA-Drop data (red) exhibit multiple TADs. RNAPII ChIA-Drop data (green) are abundant in RAIDs (blue bars). *Below*, inter-RAID RNAPII ChIA-Drop complexes are displayed and fluorescent DNA probe R1, R2, R3 and R4 are indicated.

d. FISH images of 4-color probes. *Left*, 4 probes colocalized in normal cells (Norm) in 27 of 213 nuclei in two replicates. *Right*, 4 probes were scattered in heat-shock (HS) cells in 144 of 150 nuclei in two replicates.

e. FISH colocalization percentages (Norm, $n=213$; HS, $n=150$).

f. Histogram ranging from homogeneous (left) to heterogeneous. *Top*, RNAPII ChIA-Drop (green, n=476) and ChIA-Drop (red, n=582) complexes binned within each domain (statistic=0.95, $p<2.2\times10^{-16}$; two-sided Kolmogorov-Smirnov test). *Bottom*, heterogeneity for active promoters in each RAID in RNAPII ChIA-Drop (green, n=427) and single-cell scRNA-seq (yellow, n=403) (statistic=0.27, $p=2.4\times10^{-13}$; two-sided Kolmogorov-Smirnov test).

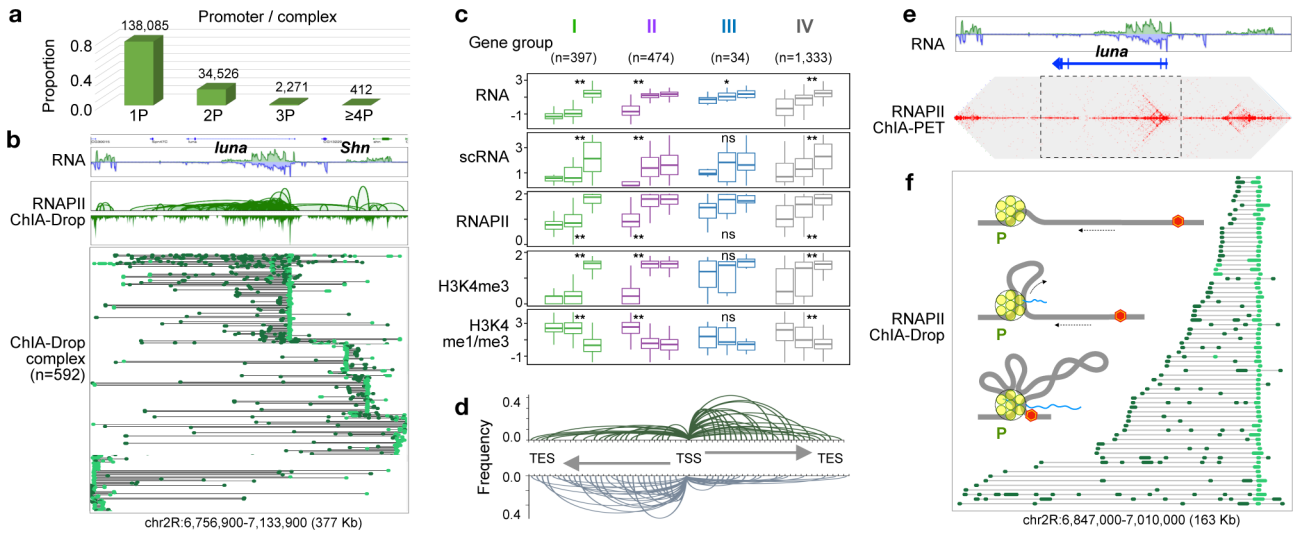

Figure 4. Promoter-centered multiplex chromatin interactions reveal topological insights for transcription.

a. Proportion of chromatin complexes involving one promoter (1P) or more (2P, etc.).

b. Browser view of a chr2R segment. RNAPII ChIA-Drop promoter (bright-green)-linked chromatin complexes (*n*=592) are depicted with non-promoter fragments (dark-green).

c. Four subtypes of 3-promoter (3P) chromatin complexes were identified based on expression levels of the three corresponding genes. Three boxplot columns for each group correspond to these three genes involved in each complex (boxplot: middle line, median; box, interquartile range (IQR); whiskers, 1.5xIQR). Two-sided Kruskal–Wallis test yields 'ns': $p>0.05$; *: $p\leq0.05$; **: $p<2.2\times10^{-16}$ for 2,238 genes involved in 3Ps. The y-axes units: "expression RPKM" (RNA), "cell count" (scRNA), "max coverage" (RNAPII, H3K4me3), and "ratio" (H3K4me1/me3).

d. Aggregation plot of RNAPII ChIA-Drop data showing average chromatin contact profile over all active genes (plus strand: green; minus strand: gray).

e. RNAPII ChIA-PET data in the *luna* gene shows a chromatin contact "stripe" from the promoter into the gene body.

f. RNAPII ChIA-Drop complexes involving *luna* promoter (*n*=72). Inset: a one-sided extrusion model for chromatin looping for transcription initiation and extension. RNAPII (yellow circles); promoter (P); DNA (gray line); moving direction (arrow); TES (red hexagon); transcript (blue wavy line).